ARTICLE

Clinical Research

Characterization of a castrate-resistant prostate cancer xenograft derived from a patient of West African ancestry

Brendon M. Patierno[1], Wen-Chi Foo[2,3], Tyler Allen[2], Jason A. Somarelli[1,2], Kathryn E. Ware[1,2], Santosh Gupta[1,2], Sandra Wise[4], John P. WiseSr.[4], Xiaodi Qin[2], Dadong Zhang[2], Lingfan Xu[3], Yanjing Li[3], Xufeng Chen[3], Brant A. Inman[2,5], Shannon J. McCall[2,3], Jiaoti Huang[2,3], Rick A. Kittles[6], Kouros Owzar[2,7], Simon Gregory[1,2,8], Andrew J. Armstrong[1,2,5,9], Daniel J. George[1,2,5], Steven R. Patierno[1,2], David S. Hsu[1,2,8,10] and Jennifer A. Freedman[1,2,10]✉

BACKGROUND: Prostate cancer is a clinically and molecularly heterogeneous disease, with highest incidence and mortality among men of African ancestry. To date, prostate cancer patient-derived xenograft (PCPDX) models to study this disease have been difficult to establish because of limited specimen availability and poor uptake rates in immunodeficient mice. Ancestrally diverse PCPDXs are even more rare, and only six PCPDXs from self-identified African American patients from one institution were recently made available.

METHODS: In the present study, we established a PCPDX from prostate cancer tissue from a patient of estimated 90% West African ancestry with metastatic castration resistant disease, and characterized this model's pathology, karyotype, hotspot mutations, copy number, gene fusions, gene expression, growth rate in normal and castrated mice, therapeutic response, and experimental metastasis.

RESULTS: This PCPDX has a mutation in *TP53* and loss of *PTEN* and *RB1*. We have documented a 100% take rate in mice after thawing the PCPDX tumor from frozen stock. The PCPDX is castrate- and docetaxel-resistant and cisplatin-sensitive, and has gene expression patterns associated with such drug responses. After tail vein injection, the PCPDX tumor cells can colonize the lungs of mice.

CONCLUSION: This PCPDX, along with others that are established and characterized, will be useful pre-clinically for studying the heterogeneity of prostate cancer biology and testing new therapeutics in models expected to be reflective of the clinical setting.

Prostate Cancer and Prostatic Diseases; https://doi.org/10.1038/s41391-021-00460-y

INTRODUCTION

Significant disparities in prostate cancer (PCa) incidence and mortality exist among racial/ethnic groups, as the age-adjusted incidence and mortality rates for PCa among African American men are 1.7- and 2.3-fold greater, respectively, compared with white men [1–3]. Such racial disparities likely result from a complex interplay among social, lifestyle/environmental, health system, and biological determinants of health [4–6]. To model race-related aggressive PCa and develop therapeutic agents against it, preclinical models derived from PCas from racially/ethnically diverse patients are required. To date, the MDA PCa 2b cell line is the only non-virally transformed PCa cell line derived from a patient of West African ancestry [7], and only recently were the first six patient-derived xenograft (PDX) models of PCa from self-identified African American patients established [8].

Researchers have begun to use patient-derived models of PCa to study the molecular basis of PCa subtypes and develop new therapeutics [9–23]. PCa PDX (PCPDX) models have been reported; for example, Lawrence et al. reported ten PCPDXs established largely from metastases from patients who had undergone treatment with enzalutamide, and showed efficacy of ribosome targeting therapeutics against these PCPDXs [21]. Other studies have shown that explant and xenograft models of androgen independent PCa closely recapitulate immunostaining and RNA-sequencing profiles of clinical CRPC specimens [7, 22]. PCPDXs have been difficult to establish, as they do not readily grow in the flank of immunodeficient mice, and mouse prostates have a limited capacity to house and grow tumors [11]. For example, in a recent study by the Novartis Institute for Biomedical Research, which presented the generation of 1075 PDXs representing a

[1]Department of Medicine, Division of Medical Oncology, Duke University School of Medicine, Durham, NC 27710, USA. [2]Duke Cancer Institute, Duke University School of Medicine, Durham, NC 27710, USA. [3]Department of Pathology, Duke University School of Medicine, Durham, NC 27710, USA. [4]Department of Pharmacology and Toxicology, University of Louisville School of Medicine, Louisville, KY 40202, USA. [5]Department of Surgery, Duke University School of Medicine, Durham, NC 27710, USA. [6]Division of Health Equities, Department of Population Sciences, City of Hope, Duarte 91010 CA, USA. [7]Department of Biostatistics and Bioinformatics, Duke University School of Medicine, Durham, NC 27710, USA. [8]Center for Genomics and Computational Biology, Duke University, Durham, NC 27710, USA. [9]Department of Pharmacology and Cancer Biology, Duke University, Durham, NC, USA. [10]These authors contributed equally: David S. Hsu, Jennifer A. Freedman. ✉email: jennifer.freedman@duke.edu

Received: 15 April 2021 Revised: 31 August 2021 Accepted: 15 September 2021
Published online: 13 October 2021

range of different tumor types, no PCPDXs were reported [10]. Attempts to improve PCa uptake in mice have included using tissue slice grafts to maximize tumor composition, supplementation with testosterone, and implantation under the renal capsule to maximize vascularization [11, 12, 15] Other methods to develop preclinical models of PCa include a recent study using metastatic foci from tissue acquisition necropsy to generate 21 PCPDXs, designated the LuCAP series [20]. These represent PCas from a spectrum of metastatic sites and are derived from patients of unknown ancestry [20]. The LuCAP series have been continually passaged in hosts rather than stored as frozen stock, and models in this series have a range of take rates when grafted into a new host, with a reported average take rate of 10%. As aforementioned, Palanisamy et al. recently reported establishment of 154 PDXs derived from 99 PCa patients, with take rates between 20% to 30%, including 47 that they have characterized and that can be expanded as cell lines (MDA PCa 2a and 2b) or PDXs [8]. The PCPDX models are from 88 self-identified Caucasian patients, 6 self-identified African American patients, and 5 self-identified Hispanic patients. Estimated ancestry was not reported.

Herein, we established a PCPDX model using malignant prostate tissue from a patient of estimated 90% West African ancestry. We demonstrated successful engraftment of this PCa back into mice after liquid nitrogen freeze with a 100% take rate. In addition, we characterized this PCPDX, including pathology, karyotype, hotspot mutations, copy number, gene fusions, gene expression, growth rate in normal and castrated mice, therapeutic response, and ability to colonize the lungs in vivo after tail vein injection.

MATERIALS AND METHODS

Human PCa specimens

Between 2014 and 2017, 230 men undergoing surgery for PCa consented to have some of their prostate tissue harvested for research by the Duke BioRepository & Precision Pathology Center (BRPC) under Duke IRB protocol 00035974. Tissue from 189 of these patients was transferred and used for research including PCPDX development under Duke IRB protocol 00079652. Transferred samples were de-identified (all 18 HIPAA identifiers removed), and only a limited set of clinical information (age, gender, self-identified race, ethnicity, pathologic diagnosis, surgical procedure performed, prior treatment history) was provided with the samples.

PCPDX generation

All animal studies were performed under a Duke University Animal Care and Use Committee (IACUC) approved protocol and PDXs were developed, as previously described [16, 17]. Briefly, surgical pathology created frozen Optimal Cutting Temperatures (OCTs) from prostate samples, which were then cut, mounted on slides, and stained. Following a pathological review of the slides, areas of tissue having the highest tumor content were released in minimal media for PCPDX generation. This process ensured higher tumor content in the samples used and ensured samples were implanted ~95 min or less after termination of blood flow. Tissues were then washed with phosphate buffered saline (PBS) and then minced into pieces ~2 mm in size and injected into the flanks of 8–10-week-old JAX NOD.CB17-PrkdcSCID-J (SCID) or NOD.Cg-*Prkdc*^{scid} *Il2rg*^{tm1Wjl}/SzJ (NSG) mice obtained from the Duke University Rodent Genetic and Breeding Core to develop subcutaneous tumors.

For the development of sub-renal capsule tumors, 8–10-week-old JAX NOD.CB17-PrkdcSCID-J or NOD.Cg-*Prkdc*^{scid} *Il2rg*^{tm1Wjl}/SzJ mice were placed in a left lateral decubitus position and the fur clipped at the site above the left kidney. The fur-clipped surgical site was prepared with a disinfectant scrub followed by an alcohol derivative three times. A small incision was made in the left flank and extended through the fascia to enter the peritoneal cavity. The kidney was displaced outside the peritoneum and the capsule was then lifted up above the kidney using forceps to create a small space between the kidney and capsule. An ~2 mm^3 specimen was then inserted into the space using a plastic 10 µL Gilson pipette tip. The specimen was pushed far enough so that it remained stably within the capsule and the hole in the capsule could be cauterized without damaging the specimen. The kidney was placed back into the peritoneum and the wound in the peritoneum was then sutured closed. Lymphomas have been known to occur in these animals around approximately six months; therefore, mice were checked daily for initial growth and observed for a total of four months. If growth was observed beneath the implantation site, the hair surrounding the tumor was cut with clippers and the skin was sterilized with ethanol so that tumors could be carefully measured with OSHLUN electronic calipers.

Mice were sacrificed once tumors exceeded 10 × 10 mm and tissue was harvested at 150 mg/mL in PBS for serial passaging and for testing therapeutic response. To test therapeutic response, tissue was dissociated with the MACS GentleMACS Dissociater and 200 µL of the suspension, ~10^8 cells, was injected into each new mouse with a 19-guage needle.

Histology

Surgical specimens were collected and formalin-fixed, paraffin-embedded (FFPE) for standard histological evaluation by Hematoxylin and Eosin (H&E). Additional 4 µM sections were used for immunohistochemistry (IHC) to confirm the diagnosis and characterize the PCa. 4 µM sections were also cut from FFPE blocks of the PDX specimen for standard histological evaluation by H&E and characterization by IHC. The antibodies used for immunohistochemical characterization were CK8/18 (Dako, 1:200), Pin-4 (combination of p63 (Dako, 1:100), CK34BE12 (Dako, 1:25), and P504S (Dako, 1:50)), PSA (Dako, RTU), PAP (Leica, 1:200), Synaptophysin (Leica, RTU), Chromogranin (Leica 1:200), NSE (Leica, RTU), Ki-67 (Leica, 1:50), CK34BE12 (Dako, RTU), and Derm CK (combination of AE1/3 (Leica, 1:800), Cam 5.2 (Leica, 1:100), and MNF116 (Leica, 1:400)).

Karyotype

Karyotype analysis was performed using logarithmically growing cells, arrested at metaphase using colchicine, and cells were harvested using standard methods for chromosomal analysis [24]. Briefly, cells were collected by trypsinization, pelleted, and re-suspended in 0.075 M KCl followed by fixing with methanol:acetic acid (3:1). Cells were dropped onto clean wet slides and aged for 45 min in a 90 °C oven. Metaphases were Giemsa-banded, and 30 metaphases were karyotyped.

Ancestry estimate

Global genetic ancestry analysis was performed as previously described [25]. Briefly, DNA was genotyped for 100 ancestry informative markers (AIMs) using the Sequenom MassARRAY iPLEX platform. The AIMs panel consisted of carefully selected autosomal markers previously identified and validated for estimating continental ancestry information in admixed populations. Individual single-nucleotide polymorphism (SNP) genotype calls were generated using Sequenom TYPER software. Individual admixture estimates for the patient were calculated using a model-based clustering method as implemented in the program STRUCTURE v2.3. Given uncertainty regarding the ancestry of the sample, the admixture model was used to determine which estimation of K (number of sub populations) was the best fit for the data. K was set from 2 to 5 and 100 iterations were run. $K = 3$ was determined to have the best fit and was used in generating estimates.

Copy number alterations

To investigate genome-wide copy number alterations, an array comparative genomic hybridization (CGH) experiment was conducted on PCPDX DNA samples in duplicates. Array CGH was a two-color based method, where PCPDX DNA was labeled with Cyanine-3 (Cy5)-dUTP and reference DNA with Cyanine-3(Cy3)-dUTP, and hybridized together. Male genomic DNA from a healthy individual was used as a reference control for aCGH hybridization (SureTag DNA Labeling Kit, Cat#5190-3400). Agilent SurePrint G3 Human CGH array (60-mers, 4X180K, Cat#G4449A, Agilent Technologies, CA, USA) containing about 170,334 Distinct Biological Features spotted on the array chip with an estimated 13Kb overall median probe arrangement (hg19), and an ~5–10 Mb copy-neutral loss of heterozygosity resolutions was used. After 24 h of hybridization and washing (Cat#5188-5226, Agilent OligoCHG Wash Buffers), slides were scanned in an Agilent Scanner C. Raw data was uploaded in Agilent CytoGenomics Software and analyzed for the detection of genomic copy gains or losses. Further, to reduce false-positives, stringent filtering criteria were applied by using a minimum three probes to call a copy gain or loss, and an average absolute

log2 ratio for gain ≥0.25 and loss <−0.25 was used. Additionally, all genomically altered genes were judged manually based on probe distribution within chromosomal aberration regions analyzed in the Agilent CytoGenomics software [26].

Hotspot mutations

The Ion AmpliSeq™ Cancer Hotspot Panel v2 (CHP2) (Thermo Fisher) was used to identify hotspot mutations. This is a next generation sequencing (NGS)-based assay consisting of 207 amplicons in a single primer pool that target various cancer "hotspot" variants across ~2800 Catalogue of Somatic Mutations in Cancer (COSMIC) mutations from 50 oncogenes and tumor suppressor genes using an amplicon-based AmpliSeq library. For the CHP2 assay, sequencing was performed on the Ion Torrent Personal Genome Machine (Thermo Fisher). To identify additional gene mutations, NGS was also performed using the VariantPlex Myeloid Kit (ArcherDX), which has 75 gene targets that are frequently mutated in myeloid malignancies. The gene content partially overlaps the gene content of the CHP2 assay. Downstream sequencing was performed on the high-throughput Illumina NextSeq 500 (Illumina).

Gene expression and fusions

Total RNA was extracted from mouse tumors with the High Pure RNA Isolation Kit (Roche Life Science). The concentration and quality was assessed on a Qubit 2.0 (ThermoFisher Scientific) and a 2100 Bioanalyzer (Agilent Technologies), respectively. Illumina Truseq Stranded total RNA-seq Kit combined with ribozome (ribo-zero) and globin depletion was used to prepare total RNA-seq libraries. Total RNA was first depleted of the rRNA and Globin mRNA using biotinylated probes that selectively bind rRNA and globin species. In this protocol, strand specificity information was determined with the dUTP "marking" method. After reverse transcription, Illumina sequencing adapters were ligated to the dscDNA fragments and amplified to produce the final RNA-seq library. This protocol did not amplify the strand marked with dUTP, allowing strand-specific sequencing. Libraries were indexed using a dual indexing approach, allowing pooling of multiple libraries and sequencing on the same sequencing flow cell. Before pooling and sequencing, fragment length distribution and library quality were assessed on a 2100 Bioanalyzer using the High Sensitivity DNA Kit (Agilent Technologies). All libraries were pooled in equimolar ratio and sequenced. Libraries were sequenced on an Illumina NovaSeq 6000 sequencer. Multiplexing 24 libraries on an Illumina S2 NovaSeq flow cell yielded between 200 and 300 million 151 bp paired-end sequences per sample after combining two runs. Once generated, sequence data was de-multiplexed and Fastq files generated using Illumina Bcl2Fastq2 conversion software.

FastQC (v0.11.5) [27] and MultiQC [28] were used to assess the initial quality of the sequences stored in fastq files pre- and post-quality control. Low quality sequences and adapters were assessed and removed using Trimmomatic (v0.36-3) [29]. Sequencing reads that passed quality control were aligned to reference human genome GRCh38 using STAR aligner (v2.6.1d) [30]. The aligned reads were annotated to genomic features using HTSeq [31] implemented in the STAR program. The reference genome sequence and GTF file were obtained from GENCODE project (Release 31). Mapping rates to rRNA and intron regions were assessed using the CollectRnaSeqMetrics tool from Picard v2.13.2 accessed 10-3-2017 (http://broadinstitute.github.io/picard).

Potential tissue contamination from mice was assessed using several strategies based on five selected samples (including two of the PDXs from mice treated with enzalutamide, one PDX from a mouse treated with the vehicle (treatment control), as well as two primary human cell populations, which served as negative controls with no mouse tissue present). The assessment strategies included: different resources of reference genome assemblies: GENCODE GRCh38 primary assembly and UCSC GRCh38 assembly; different versions of STAR aligner [30]: v2.5.4b and v2.6.1d; using human and mouse combined reference genomes: GENCODE GRCh38 primary human genome + GENCODE GRCm38 primary mouse genome; UCSC GRCh38 human genome and UCSC GRCm38 mouse genome; different settings for STAR aligner arguments: outFilterMatchNminOverLread and outFilterScoreMinOverLread with 0.33, 0.5 or 0.66 (default).

Gene differential expression was performed within the framework of a negative binomial model using the R (v3.5.3) [30] and its extension package DESeq2 (v1.20.0) [31]. All statistical analyses were adjusted for multiple testing within the framework of control of the false-discovery rate, unless stated otherwise [32–34].

Gene fusion candidates were analyzed using STAR-Fusion (v1.6.0) [35]. The gene fusion reference library was obtained from the Broad Institute pre-built CTAT library: GRCh38_gencode_v29_CTAT_lib_Mar272019.plug-n-play.tar.gz accessed 04-02-2019 (https://data.broadinstitute.org/Trinity/). The fusion results were visualized using R package chimeraviz v1.10.0 [36]. Statistical analyses were mainly scripted using the R statistical environment [37] along with its extension packages from the comprehensive R archive network (CRAN; https://cran.r-project.org/) and the Bioconductor project [38]. The analyses were carried out with adherence to the principles of reproducible analysis using the knitr package [39] for generation of dynamic reports. All analyses were programmed and documented on 04/02/2019 using mercurial (https://www.mercurial-scm.org/) for source code management and are available through a non-commercial source code repository (https://gitlab.oit.duke.edu/dcibioinformatics/pubs/hsu-pc-pdx-rnaseq) (Gitlab registered account required).

Therapeutic response

Drug sensitivity studies on the PCPDX were performed as follows. Mice from the second passage of the original PDX were sacrificed once tumors exceeded 10 × 10 mm and tissue from multiple tumors were harvested at 150 mg/mL in PBS for serial passaging and for testing therapeutic response. To test therapeutic response, tissue from multiple tumors was dissociated with the MACS GentleMACS Dissociater, and 200 µL of the resulting suspension, ~10^8 cells, was injected into the flanks of each JAX NOD.CB17-PrkdcSCID-J mouse. Growth was monitored until the tumors measured ~100–150 mm^3. Mice were then randomized into 6 groups: enzalutamide ($n = 5$), control 1 (DMSO) ($n = 5$), castration surgery ($n = 5$), control 2 (DPBS) ($n = 5$), docetaxel ($n = 5$) and cisplatin ($n = 5$). All of the mice in each group were used to assess tumor growth in each condition. To perform blinded assessments for tumor measurements, a second technician was given cages of mice without seeing cage number or marking and this technician measured the tumor volume. For RNA-sequencing analysis, RNA was isolated from the tumors of 3 mice from each drug treatment and respective vehicle control groups. RNA-sequencing data from the castration surgery group is not shown.

Enzalutamide, docetaxel and cisplatin were acquired from the Duke University Pharmacy stockroom. Enzalutamide was diluted in 1:20 DMSO in ultrapure distilled water and delivered at 10 mg/kg by oral gavage five times per week. Docetaxel was diluted in 1:20 DMSO and cisplatin was diluted in DPBS and administered by intraperitoneal injection twice per week at 8 mg/kg and 3.5 mg/kg, respectively as standard doses [23].

Experimental metastasis

To establish an experimental metastasis model, tumor samples were homogenized and filtered through a 30 µM and then 10 µM filter, suspended in PBS, and injected into the tail veins of NSG mice at a density of 5×10^5/200 µL using a 30G1/2 needle and a 1-mL syringe. A total of 10 weeks after injection the animals were sacrificed. The lungs were removed, rinsed in PBS, and fixed in 10% neutral buffered formalin. Whole lungs were sectioned and stained with hematoxylin and eosin (H&E) according to routine protocols, and a genitourinary pathologist performed histological evaluation.

RESULTS

Patient clinical history

Clinical history of the patient showed that he was initially diagnosed with Gleason pattern 5 + 5 = 10 prostate adenocarcinoma. He was then treated initially with external beam radiation therapy and did well until seven years later when his PSA began to rise (Fig. 1). Following this biochemical recurrence, he was started on combined androgen blockade with bicalutamide (non-steroidal androgen receptor inhibitor) and goserelin (luteinizing-hormone releasing hormone (LH-RH) agonist). Six years later, his PCa became castrate-resistant and his PSA rose to 3.1 ng/ml. Imaging demonstrated bone metastases in the ribs and pelvis and he began treatment with abiraterone and prednisone. Within two months, his PSA dropped to 0.83 ng/mL and soon thereafter, he was started on denosumab as bone-directed therapy for his bone metastases.

Within another month, it was determined this high-grade PCa required a pelvic exenteration. At pelvic exenteration, the tumor had entirely replaced the prostate, and demonstrated invasion into the seminal vesicles, bladder and rectal wall. The rectal mucosa was uninvolved. There was also evidence of angioinvasion and perineural invasion and 3/17 regional lymph nodes contained tumor. The patient's disease stage was pT4N1Mx. The sample used to establish the PCPDX was taken from this procedure from malignant prostate tissue.

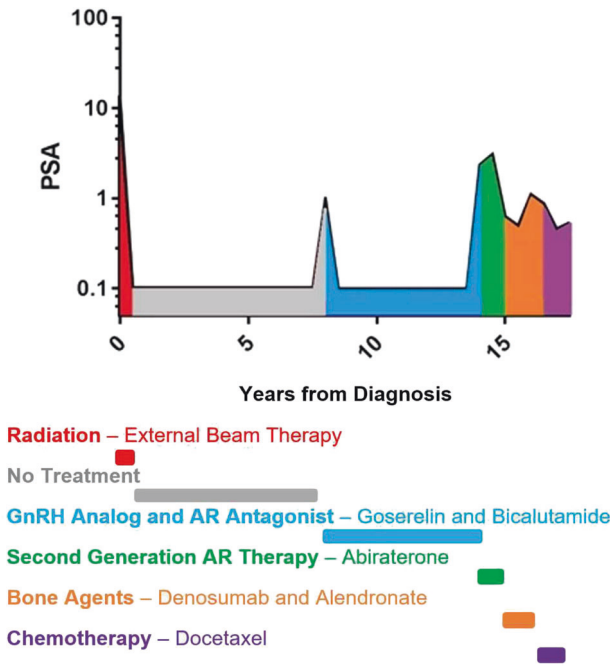

Fig. 1 Patient clinical history. Patient PSA during years from diagnosis and treatment history. The patient initially had an elevated PSA, which dropped and remained <3.1 after radiation therapy. After a period of response to radiation therapy, his PSA increased and his prostate cancer progressed to advanced CRPC. Before attainment of the surgical specimen used to generate the PCPDX, the patient had failed radiation therapy, androgen deprivation therapy, secondary hormonal therapy, denosumab, alendronate, and chemotherapy.

Generation of the PCPDX

From 2014-2017, 189 patients undergoing surgery for their PCa were identified and, after the surgical procedure, prostate tissue cores were collected for the establishment of PCPDXs. The majority of samples were from patients undergoing radical prostatectomy, and we collected data on race and PSA levels for these patients (Supplementary Table 1). We also recorded the attempts at PDX formation, including mouse line, number of mice used, and site of implantation (Supplementary Table 1). The vast majority of these cases were Gleason Grade 6-7 adenocarcinomas, and only one patient had high-grade disease. A total of 41% of the prostate tissue cores were grafted into NOD.SCID mice and 59% were grafted into NSG mice. From the 189 samples injected, we generated one PCPDX for an overall take rate of 0.52%. This PCPDX was generated from a specimen grafted into a NSG mouse under the renal capsule, without testosterone supplementation. Our standard operating procedure (SOP) for generation of PDXs required freezing a portion of each PDX tumor for the first three passages to generate fresh frozen vials of PDX for future PDX generation. Per our SOP, we tested the viability of the fresh frozen stock starting at the third passage to re-generate PDX and for this PDX, the rate of regeneration from fresh frozen stock was 100% (10/10). Growth can be detected in these PDXs after just two weeks, and tumors will reach 1000 mm^3 in the following 15–20 days. Two subsequent generations were implanted, and we observed growth rates in the same range as well as homogenous histology between the generations.

Patient and PCPDX histology

Histological evaluation of the patient's tumor revealed a poorly differentiated malignancy arranged in solid sheets without obvious glandular formation. Tumor cells exhibited pleomorphic nuclei, prominent nucleoli, and increased mitoses. Large areas of geographic necrosis were readily identified (Fig. 2). A wide panel of immunohistochemical stains showed the tumor to be consistent with a highly de-differentiated PCa (Table 1). Epithelial stains (cytokeratin cocktail, CK8/18, CK34bE12) were only focally positive while many prostate lineage specific markers (NKX3.1, PSA, PAP, and P501S) were negative. Racemase, which is expressed in the majority of PCas, was focally positive in this tumor. Stains for neuroendocrine differentiation (synaptophysin, chromogranin, NSE) and androgen receptor were also negative. The tumor showed a moderately high proliferation index by Ki-67. The tumor stained negative for p63, excluding urothelial carcinoma.

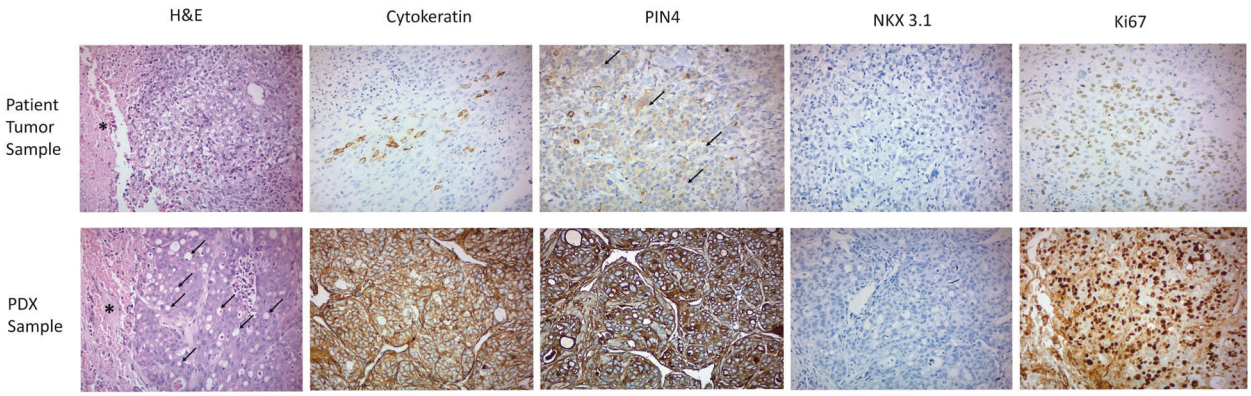

Fig. 2 Patient and PDX immunohistochemical profiles. H&E staining at 20× magnification of the patient's tumor and the established PDX both demonstrate pleomorphic nuclei with prominent nucleoli, as well as areas of geographic necrosis (*). The patient tumor cells are arranged in solid sheets with no obvious glandular differentiation, whereas the PDX cells are arranged predominantly in nests with scattered luminal structures (arrows). Immunohistochemical staining shows patient and PDX tumor cells to be negative for NXK3.1, PSA and PAP. A small number of cells in the patient tumor specimen stained positive for cytokeratin, with intermittent cells staining positive for Ki-67. The PCPDX model stained much more diffusely positive for cytokeratin, with many cells staining strongly for Ki-67. The patient tumor specimen shows tumor cells to be focally positive for racemase (cytoplasmic stain, red chromogen) (arrows), with rare cells expressing CK34bE12. The PCPDX stains negative for racemase, and stains diffusively positive for CK34bE12.

Table 1. Patient tumor and PCPDX immunohistochemical staining.

Stain	PDX	Patient
Cytokeratin cocktail	Strong and diffusely positive	Focally positive
CK8/18	Strong and diffusely positive	Focally positive
PIN4	Diffusely CK34be12 positive	Focally positive for racemase and CK34bE12
PSA	Negative	Negative
NKX 3.1	Negative	Negative
PAP	Negative	Negative
P501S	Negative	Negative
AR	Negative	Negative
GR	Negative	Positive
Synaptophysin	Negative	Negative
Chromogranin	Negative	Negative
NSE	Negative	Negative
Ki-67	High	Moderately high

A panel of immunohistochemical stains were performed on the clinical and PCPDX specimens. The first column indicates the IHC stain being used, and the second and third column indicate the staining results in either the PDX or patient sample respectively. Cytokeratin stains confirm the epithelial lineage of the tumor. Prostatic lineage markers such as NKX 3.1, PSA and PAP negative staining indicate a highly de-differentiated cancer. A cocktail of antibodies performed on the clinical specimen showed tumor cells to be focally positive for racemase (cytoplasmic stain, red chromogen) and CK34bE12 (cytoplasmic stain, brown chromogen). The PCPDX has a similar IHC profile as well as shares specific features from certain cells in the patient tumor specimen, despite colonization and propagation in mice.

Similar to the patient tumor, the PCPDX showed pleomorphic tumor cells with prominent nucleoli and areas of geographic necrosis (Fig. 2). Tumor cells were arranged predominantly in nests, but scattered luminal structures were present, consistent with glandular differentiation. Immunohistochemical staining showed strong and more broadly positive staining for epithelial markers by cytokeratin cocktail, CK8/18 and CK34bE12 in the PCPDX, but prostatic lineage specific markers such as NKX3.1, PSA, PAP and P501S were negative, consistent with what we observed in the original patient's tumor (Fig. 2 and Table 1). Stains for racemase, p63, AR, and neuroendocrine markers synaptophysin, chromogranin and NSE were also all negative. The Ki-67 stain was diffusely positive indicating a high level of proliferation.

Patient ancestry and karyotype of the PCPDX

Ancestral genotyping of DNA from the patient revealed estimated 90% West African, 7% Native American, and 2% European ancestry for this self-identified African American patient. Notably, after three passages, the PCPDX had similar estimated ancestry, with estimated 88% West African, 9% Native American, and 3% European ancestry (Supplementary Table 2).

Karyotype analysis on a total of 30 PCPDX cells showed an extra Y chromosome, additional material on chromosome 8, and deletion of material on chromosome 9 (arrows indicate abnormal chromosomes) (Fig. 3A). Two cells also had deletion of material on chromosome 20 (data not shown). ISCN designation: 47, XYY, add (8) (p23), del (9) (p22) [28]. Additional non-clonal abnormalities were observed in four cells; one cell had additional material on chromosome 9q, one cell had a deletion in chromosome 11q, one cell had a deletion in chromosome 13q, one cell had additional material on chromosome 4, a deletion in chromosome 6p, and a deletion in chromosome 7p (Supplementary Fig. 1).

Genomic characterization of the PCPDX

We first performed next generation sequencing using two hotspot mutation assays to screen the PCPDX sample for mutations shown previously to be drivers of PCa (Table 2). Both screens detected a frameshift mutation in TP53 (NM_000546.5:c.1005_1008delTGAG). Neither assay detected reads for PTEN or RB1, which is highly suggestive of deletions involving these genes.

We next performed copy number analysis of the PCPDX (Table 3). Genome-wide analysis revealed 660 genes with copy number alterations (Supplementary Table 3). Pathway analysis of this gene list using Gene Annotation Tool to Help Explain Relationships (GATHER) showed the three most significant pathways affected to be "response to virus, response to biotic stimulus, and defense response" (Supplementary Table 4) [40].

Consistently, Ingenuity Pathway Analysis showed almost every significant pathway alteration related to immune cell development, communication, and trafficking (Supplementary Tables 5 and 6) [41]. The PCPDX showed several important copy number alterations, including loss of *UDP Glucuronosyltransferase Family 2 Member B17* (*UGT2B17*) and *Phosphodiesterase 4D Interacting Protein (PDE4DIP)*. Loss of UDP glucuronosyltransferase family 2 members, including *UGT2B17*, have been reported as sufficient to restore free dihydrotestosterone, sustained androgen signaling, and development of castration resistance [42, 43]. A recent study reported *PDE4DIP* loss appears often in circulating tumor cells taken from men with mCRPC [26]. *Phosphatase and tensin homolog (PTEN)*, *Retinoblastoma-Associated Protein (RB1)*, and *Friend Leukemia Integration 1 Transcription Factor* (*FLI1*) loss have all been shown to be important in PCa progression [44–46]. *Gain of G Protein Nucleolar 3* (*GNL3*) has been correlated with PCa metastasis, and *SRY-Box Transcription Factor 2 (SOX2)* is often upregulated in PCa leading to metastasis and chemotherapy resistance [45–47].

Finally, we used RNA-seq data to identify gene fusions (Fig. 3B). Using this method, we did not detect the *TMPRSS2/ERG* fusion, found in ~50% of PCas [2]. Studies have reported that this fusion is less prevalent in patients of African ancestry and all of the PCPDXs derived from self-identified African American patients were reported to be ERG negative [8, 48]. We did detect snoRNA and ribonuclease-associated RNA (*RMRP* and *RPPH1*) fusions, which have been determined to play a role in PCa progression [49].

Therapeutic response of the PCPDX

To compare drug efficacy in the PCPDX and patient, we treated the PCPDX by physical castration and with enzalutamide to determine if the PCPDX, like the patient tumor, was castrate-resistant and resistant to secondary hormonal therapy. We also sought to gain insight from RNA Seq data from enzalutamide treated PDXs regarding gene expression and enzalutamide resistance. As shown in Fig. 4A, the PCPDX demonstrated primary resistance to both physical castration and enzalutamide. As a control, we treated a group of mouse tumors established from LNCaP cells with the same dose of enzalutamide, and tumor growth was completely inhibited in these experiments (data not shown). Figure 4C shows the response of individual tumors in each group.

Docetaxel remains a standard chemotherapy for treatment of advanced PCa, and this patient previously received this treatment. Therefore, we evaluated the PCPDX response to docetaxel (8 mg/kg) and saw a trend of tumor growth inhibition, but not a significant decrease in tumor volume (Fig. 4B).

Finally, to determine sensitivity of refractory disease, we treated the PCPDX with cisplatin. Cisplatin is an alkylating agent that binds to DNA bases causing cross-links and breaks in DNA strands, thus interfering with DNA replication [50], and is widely used clinically in castrate-resistant PCa. The PCPDX treated with cisplatin revealed significant tumor growth inhibition (Fig. 4), suggesting efficacy of cisplatin in this castrate-resistant, docetaxel-resistant

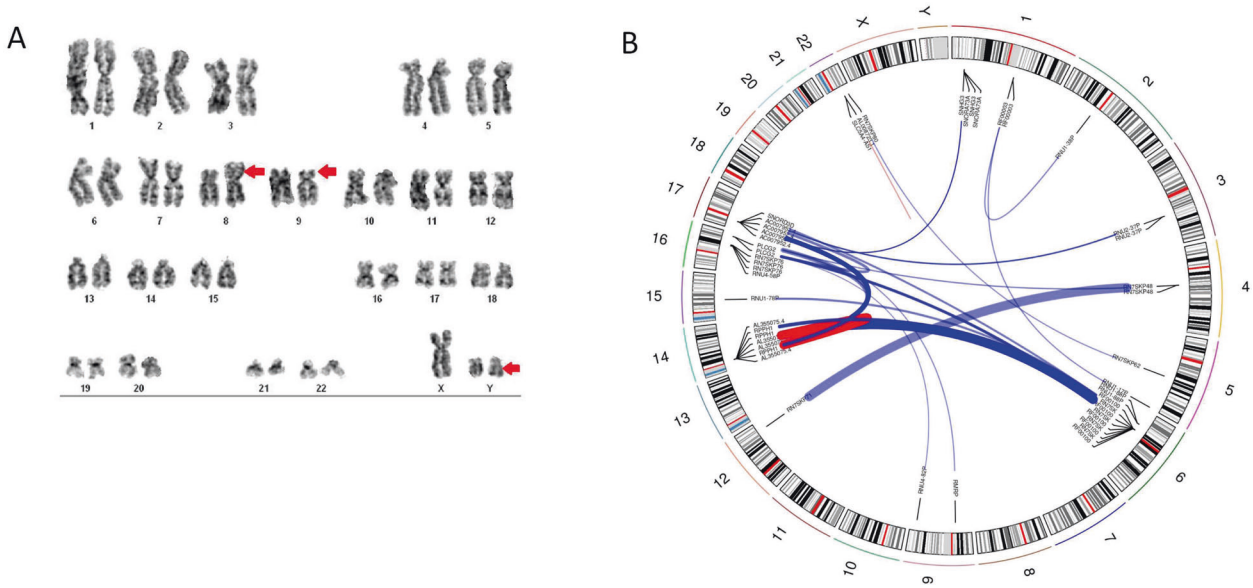

Fig. 3 PCPDX DNA and RNA analysis. A Karyotype analysis on a total of 30 PCPDX cells revealed a dominant karyotype including an extra Y chromosome, additional material on chromosome 8, and deletion of material on chromosome 9 (abnormalities indicated with red arrows). Additional karyotypes are included in Supplementary Fig. 1. **B** Gene fusions in the PCPDX visualized as a circus plot, notably lacking the *TMPRSS2/ERG* fusion seen in 50% of prostate cancers.

Table 2. Hotspot mutations in the PCPDX.

Hotspot mutations gene panel	Mutation
AKT1	None
ATM	None
BRAF	None
HRAS	None
NOTCH1	None
NRAS	None
IDH1	None
PIK3CA	None
PTEN	Deletion
RB1	Deletion
TP53	Frameshift

A next generation sequencing based assay was used to screen the PCPDX sample for mutations shown previously to be drivers of prostate cancer. The first column indicates the gene and the second column indicates whether the PCPDX has a mutation in the indicated gene and, if so, the type of mutation.

Table 3. Copy number alterations in the PCPDX.

Genes	PDX copy number alterations
NRAS	Gain
CYP11B1	Gain
UGT2B17	Loss
PTEN	Loss
PHLPP1	Loss
RB1	Loss
KMT2D	Loss
KDM5D	Gain
FANCA	Gain
FLI1	Loss
NDRG1	Gain
EGFR	Loss
ETS1	Loss
CHEK2	Gain
SOX2	Gain
CD24	Gain
CD44	Loss
GNL3	Gain
ZMYM5	Gain
MAPK14	Gain

aCGH data was used to determine copy number alterations. Gain/loss in genes of interest are indicated, with genes indicated in the first column and gain/loss in the indicated gene given in the second column.

PCa. Mice treated with cisplatin maintained a healthy weight and appearance, and by the end of the treatment, tumor growth in some mice was not only inhibited, but tumor volume was beginning to decrease (Fig. 4D).

Genomic characterization of the PCPDX treated with enzalutamide, docetaxel or cisplatin

As the PCPDX was resistant to enzalutamide and docetaxel, and sensitive to cisplatin, we performed RNA sequencing from three tumors (biological replicates) from the following treatment groups: (1) cisplatin, (2) docetaxel, (3) enzalutamide, and (4) control to begin to understand the mechanism of response to these drugs. Initial analysis focused on gene expression changes between treated and corresponding control groups, and specifically examined genes previously identified to play important roles in PCa progression to advanced and metastatic disease [2, 51].

PCPDX tumors treated with cisplatin compared with the corresponding control group revealed expression changes in 3996 genes with an unadjusted p value < 0.01 (Supplementary Table 7), including downregulation of *Enhancer Of Zeste 2 Polycomb Repressive Complex 2 Subunit (EZH2)*, *Cyclin Dependent Kinase Inhibitor 1B (CDKN1B)*, and *Ras Homolog Family Member A (RHOA)*, inhibition of which have all been linked previously to

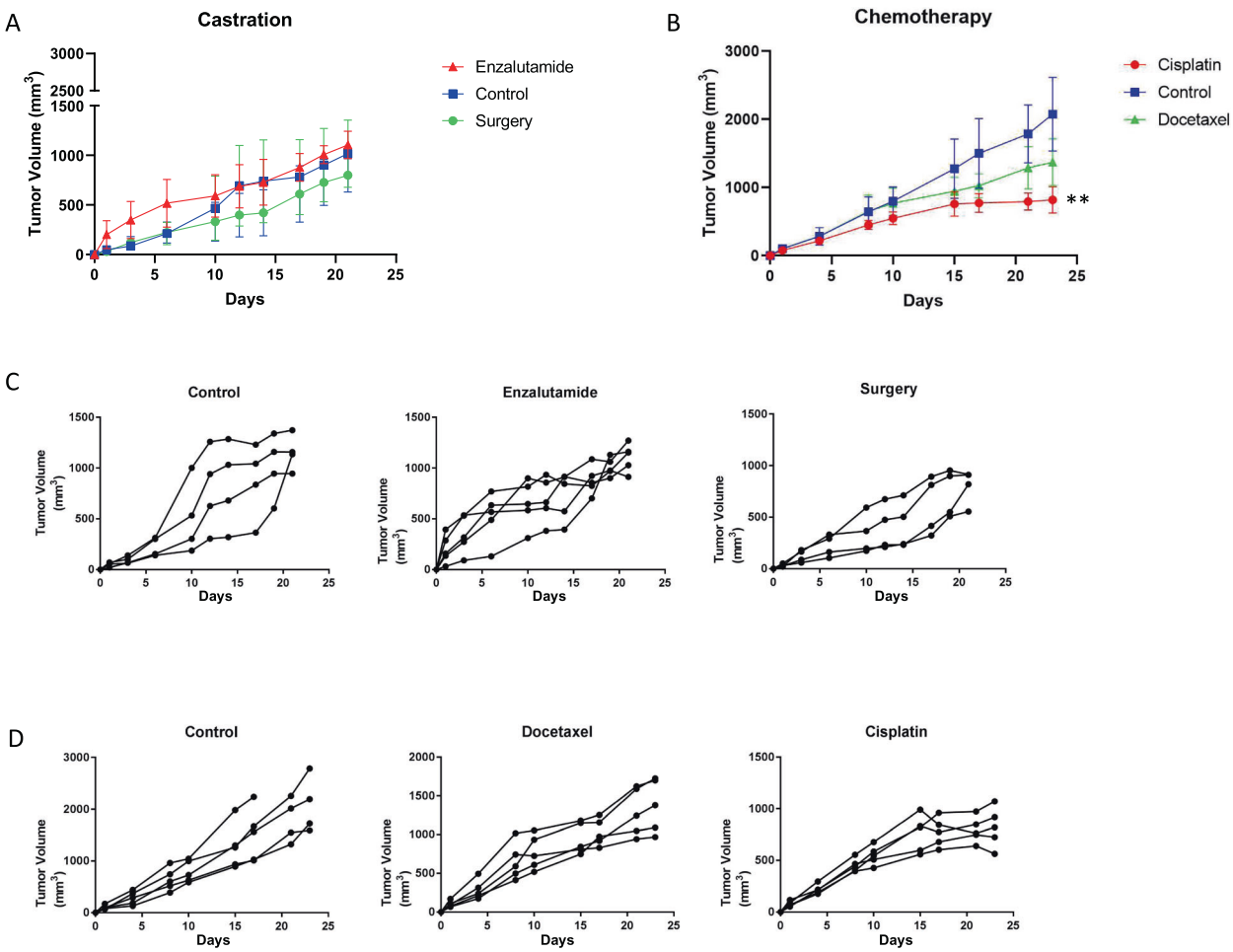

Fig. 4 Response of the PCPDX and individual PCPDX tumors to clinically relevant doses of standard-of-care prostate cancer therapies. Treatment was begun at the second measured time-point, at which point tumors had reached ~100 mm^3. An asterisk (*) indicates a statistically significant data point defined by the Holm–Sidak *t*-test (PRISM) where $^{**}P < .01$). **A** Average tumor volume over time in mice treated with enzalutamide and castration surgery versus control. **B** Average tumor volume over time of mice treated with docetaxel and cisplatin versus control. **C** Response of individual PCPDX tumors in mice from panel **A**. **D** Response of individual PCPDX tumors in mice from panel **B**.

cisplatin resistance [52–56] (Fig. 5). Ingenuity Pathway Analysis of the top 1000 genes with significant expression changes showed that the nucleotide excision repair pathway and DNA damage checkpoint regulation were significantly altered (Supplementary Table 8 and Supplementary Fig. 2).

PCPDX tumors treated with enzalutamide compared with the corresponding control group showed expression changes in 1066 genes with an unadjusted p value < 0.01 (Supplementary Table 9). Gene expression changes included upregulation of *NDRG2*, which has been associated with resistance to abiraterone and enzalutamide in PCa [57], as well as *PAX6*, which has been linked to AR transactivation and therapeutic resistance [58] (Fig. 5). In addition, *Kallikrein Related Peptidase 2* (*KLK2*) and *R-Spondin 2* (*RSPO2*) have been shown to be upregulated in advanced PCa, and both have increased expression greater than two-fold in our model in response to treatment with enzalutamide [59, 60]. Ingenuity Pathway Analysis of the top 1000 genes with significant expression changes revealed that the top pathways altered had significant effects on gastrointestinal and reproductive disease progression (Supplementary Table 10 and Supplementary Fig. 3).

PCPDX tumors treated with docetaxel interestingly did not show as many changes in gene expression when compared with the corresponding control group, with only 201 genes with unadjusted p value < 0.01 (Supplementary Table 11). Despite this, we identified upregulation of *RUNX2*, and downregulation of *NR4A1*, which both play a role in docetaxel resistance [61–64] (Fig. 5). We did not perform Ingenuity Pathway Analysis using these data, as there were not enough expression changes for robust analysis of altered pathways.

Experimental metastasis of the PCPDX

To measure the experimental metastasis [65] of the PCPDX, we injected PCPDX tumor cells into the tail veins of four NSG mice. After 10 weeks, mice were sacrificed and lungs were harvested. As shown in Fig. 6, the injection of PCPDX tumor cells resulted in metastases to the lung. For each mouse, a biopsy of the lung was obtained and two H&E slides were prepared. The whole lung was also made into a FFPE block and two H&E slides were prepared. In the lungs of four mice undergoing tail vein injections, 100% of the mice had metastatic disease (Table 4).

DISCUSSION

Herein, we established a PCPDX derived from malignant prostate tissue from a patient of estimated 90% West African ancestry. To our knowledge, this is the first PCPDX derived from a patient of estimated 90% West African ancestry and joins only six other

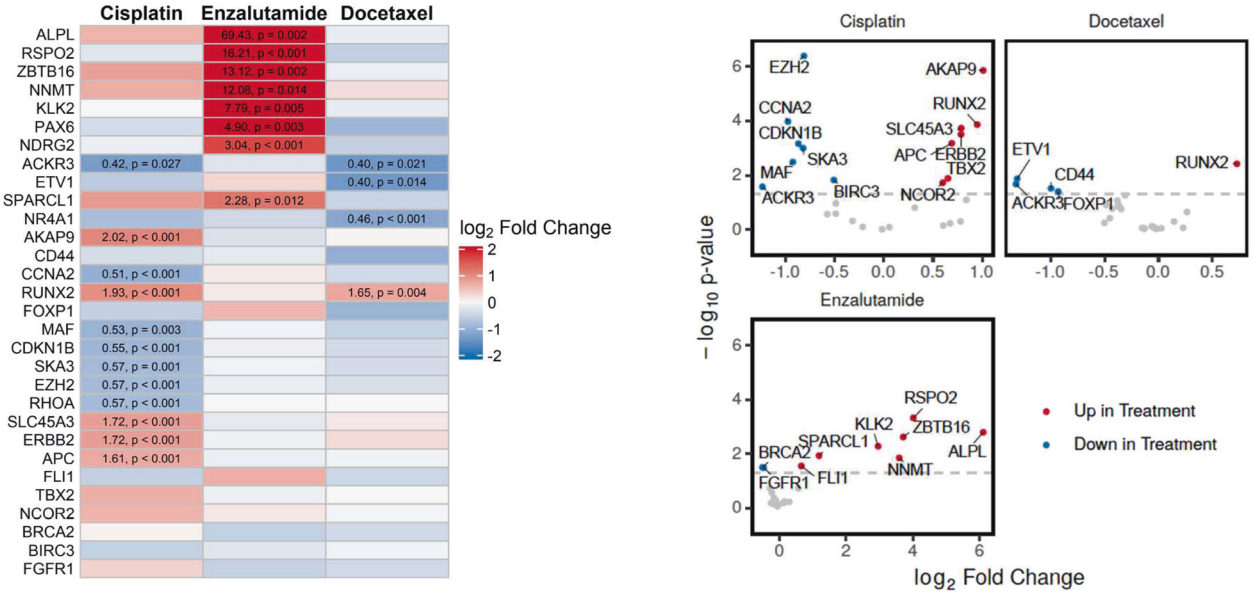

Fig. 5 PCPDX gene expression post-treatment with enzalutamide, docetaxel, or cisplatin. Heat map (left) and volcano plots (right) of fold changes in gene expression in genes of interest post-treatment with enzalutamide, docetaxel or cisplatin compared with respective controls. For the heat map, columns represent treatment groups (three mice), p value < 0.01 indicated. For the volcano plots, fold change 1.5, positive (red), negative (blue), p value < 0.01 indicated.

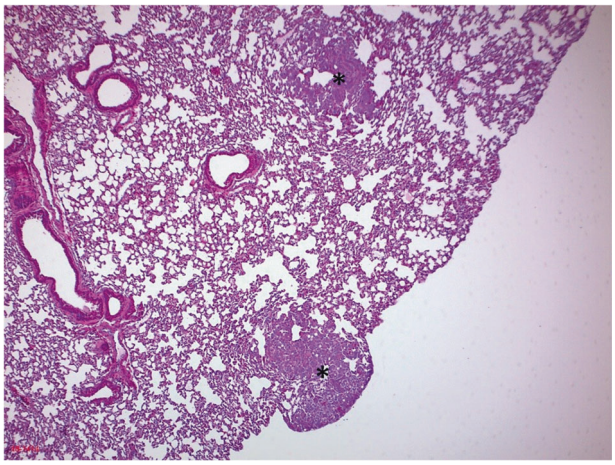

Fig. 6 H&E of mouse lung tissue with metastatic tumor foci. H&E slides were assessed at 4× magnification by a genitourinary pathologist for tumor foci, indicated by an asterisk.

Table 4. Tumor foci in mouse lungs after tail vein injections.

Sample type	Approximate # of foci	Size range (mm)	Necrosis?
Biopsy of Lung 1	2	<1–2	Y
Whole Lung 1	10	<1–1	N
Biopsy of Lung 2	2	<1	N
Whole Lung 2	1	<1	N
Biopsy of Lung 3	0	NA	NA
Whole Lung 3	2	<1	N
Biopsy of Lung 4	1	1	N
Whole Lung 4	2	<1	N

The number of, size of, and presence of necrosis in tumor foci in each sample indicated in the first column was assessed by a pathologist and indicated in the second, third, and fourth column, respectively. The whole lung was accessed as well as 2 mm^3 biopsies, which could be used for further assessment if marked positive.

PCPDXs derived from self-identified African American patients available to the PCa and the PCa disparities research community. This PCPDX is a model of castration resistant and highly treatment refractory disease and with the capacity to colonize the lungs.

From the present study and the literature, it is clear that establishing PCPDXs is extremely challenging. We found that taking samples from standard 12-hole punches of biopsies resulted in only 10% of samples containing viable tumor for implantation into immunodeficient mice, likely because PCas do not form grossly identifiable tumors and these tumors are often comprised of heterogeneous cell populations, including stroma and other normal cells. In addition, we found that higher Gleason score (8+) samples would often grow to form a nodule in the primary inoculation mice, but would not survive passaging into another mouse. Interestingly, histopathological examination of these masses revealed proliferative basal cells without evidence of invasive cancer. Furthermore, many PCPDXs established to date have low take rates and slow initial growth rates. For example, the LuCaP series of mCRPC PDXs have self-reported take rates ranging from 10% to 80%, and take 6–36 weeks to detect initial growth [20]. The PCPDX established herein is unique in that it has a 100% take rate and growth can be detected just two weeks.

Immunohistochemical staining of the patient tumor specimen confirmed a highly dedifferentiated tumor, with rare cells expressing cytokeratin. The PCPDX; however, stained highly positive for cytokeratin, confirming an epithelial lineage from the patient tumor. In addition, the PCPDX showed much stronger and more diffusely positive staining for CK34bE12 as well as Ki67. These differences between the patient tumor specimen and PCPDX staining are indicative of the tumor cell clone that was able to most effectively invade and colonize after implantation into the mouse. While further characterization of the patient tumor would have been informative, there was a limited amount of this sample available, and the available sample was exhausted during these studies. The PCPDX model represents the epithelial and highly proliferative cancer cells from the patient's heterogenous and aggressive disease. In addition,

the PCPDX stained negative for *AR*, unlike the other six PCPDXs derived from self-identified African American patients [8]. This PCPDX therefore provides a model to study loss of AR expression in the context of therapeutic resistance and disease progression in a patient of West African ancestry.

Genomic profiling and therapeutic response of the PCPDX established herein revealed insight into the biology and subtype of this preclinical model. The PCPDX has a mutation in *TP53* as well as deletions of *PTEN and RB1*. *TP53* mutation and deletion of *PTEN* and *RB1* have been linked to poor prognosis in many cancers, including PCa, and have been shown to indicate a more aggressive PCa phenotype [36, 39, 41]. These alterations were not necessarily present in the patient's primary tumor and some/all of them were likely selected for in response to treatment. While it is possible to determine exact copy number gain/loss via aCGH, we were unable to definitively count the amount of copy number gains or losses within these samples given the dynamic range of the assay. Therefore, we were unable to conclude whether deletions were hemizygous or homozygous. Deletion of *PTEN* was also reported in two of the PCPDXs derived from self-identified African American patients [8]. Importantly, the MDA PCa 2b cell line does not have mutated *TP53* or deletions of *PTEN* and *RB1* [7]. MDA PCA 2b cells are also androgen dependent and express AR as well as PSA. These differences from our model highlight the heterogeneity of PCa among patients of all races and ethnicities, and the necessity of generating models that reflect the disease at different stages and in men of all races and ethnicities. In addition, we also noted gain of *SOX2* and loss of *UGT2B17* in the PCPDX established herein, and these alterations are consistent with an advanced disease that has become resistant to secondary hormonal therapy [37, 40, 41]. Loss of *UGT2B17* was also reported in one of the PCPDXs derived from a self-identified African American patient [8]. Regarding additional copy number alterations, as in the case of this PCPDX, gain of *CYP11B1* and loss of *PHLPP1* were also each reported in one of the PCPDXs derived from self-identified African American patients [8]. Copy number alterations involving *CD24* and *MAPK14* were also identified in this PCPDX and each reported in one of the PCPDXs derived from self-identified African American patients; however, in this PCPDX both involved gain and in each of the PCPDXs derived from self-identified African American patients both involved loss [8]. Finally, we noted a number of gene fusions in this PCPDX, which have also been shown to correlate with advanced disease.

Interestingly, in contrast to the lack of response to enzalutamide and docetaxel, the tumor volume of PCPDXs treated with cisplatin significantly decreased compared with the corresponding control group. It is important to note that the PCPDX treatments were done using the same passage of the PCPDX to seed tumors, but a different piece of frozen tumor stock was used for the castration experiment and the chemotherapy experiment. Because of the difference this may have caused in the growth rates of the control groups and the small number of animals tested, we cannot make a definitive conclusion regarding the responsiveness of the PCPDX to the tested therapies. However, we observed a significant decrease in growth after treatment with cisplatin, and the corresponding RNAseq data revealed changes in genetic pathways related to DNA damage. These data suggest the potential efficacy for treatment of this tumor with cisplatin.

RNA sequencing of tumors post-treatment compared with respective vehicle control groups revealed changes in gene expression that were consistent with pathways previously reported to be altered in response to the tested therapeutics. Treatment with cisplatin resulted in decreased expression of a number of genes involved in DNA repair and cell cycle checkpoint regulation. We also observed increased expression of *PAX6, KLK2*, and *RSPO2* in response to treatment with enzalutamide, each of which have been shown to be upregulated in advanced PCa [42, 59, 60]. IPA analysis of the genes with expression changes after treatment with enzalutamide confirmed many genes were involved in advanced reproductive disease. These data suggest that the PCPDX recapitulates advanced CRPC disease, having developed the genetic networks necessary to resist treatment with enzalutamide.

The PCPDX model established and characterized herein represents late stage disease and recapitulates the biology often seen in advanced CRPC, thus providing a model of highly proliferative and drug resistant PCa with experimental metastatic potential from a patient of West African ancestry. Generation of a larger panel of PCPDXs from ancestrally diverse patients at various stages of disease will aid in development of biomarkers and therapeutic agents for aggressive PCa. Ultimately, such precision medicine interventions will reduce PCa disparities and improve outcomes for all men with aggressive PCa.

DATA AVAILABILITY

All RNA-sequencing data are available from GEO (GSE146402).

REFERENCES

1. Siegel RL, Miller KD, Jemal A. Cancer statistics, 2019. Cancer J Clin. 2019;69:7–34.
2. Cancer Genome Atlas Research Network. The molecular taxonomy of primary prostate cancer. Cell. 2015;163:1011–25.
3. Irshad S, Bansal M, Castillo-Martin M, Zheng T, Aytes A, Wenske S, et al. A molecular signature predictive of indolent prostate cancer [published correction appears in Sci Transl Med. 2013 Sep 18;5(203):203er9]. Sci Transl Med. 2013;5:202ra122.
4. Robbins AS, Whittemore AS, Thom DH. Differences in socioeconomic status and survival among white and black men with prostate cancer. Am J Epidemiol. 2000;151:409–16.
5. Pietro GD, Chornokur G, Kumar NB, Davis C, Park JY. Racial differences in the diagnosis and treatment of prostate cancer. Int Neurourol J. 2016;20:S112–S119. https://doi.org/10.5213/inj.1632722.361
6. Polite BN, Adams-Campbell LL, Brawley OW, Bickell N, Carethers JM, Flowers CR, et al. Charting the future of cancer health disparities research: a position statement from the American Association for Cancer Research, the American Cancer Society, the American Society of Clinical Oncology, and the National Cancer Institute. CA Cancer J Clin. 2017;67:353–61.
7. Navone NM, van Weerden WM, Vessella RL, Williams ED, Wang Y, Isaacs JT, et al. Movember gap1 pdx project: an international collection of serially transplantable prostate cancer patient-derived xenograft (pdx) models. Prostate. 2018;78:1262–82.
8. Palanisamy N, Yang J, Shepherd PDA, Li-Ning-Tapia EM, Labanca E, Manyam GC, et al. The MD Anderson prostate cancer patient-derived xenograft series (MDA PCa PDX) captures the molecular landscape of prostate cancer and facilitates marker-driven therapy development. Clin Cancer Res. 2020. https://doi.org/10.1158/1078-0432.ccr-20-0479.
9. Bluemn EG, Coleman IM, Lucas JM, Coleman RT, Hernandez-Lopez S, Tharakan R, et al. Androgen receptor pathway-independent prostate cancer is sustained through FGF signaling. Cancer Cell. 2017;32:474–89. e6.
10. Gao H, Korn JM, Ferretti S, Monahan JE, Wang Y, Singh M, et al. High-throughput screening using patient-derived tumor xenografts to predict clinical trial drug response. Nat Med. 2015;21:1318–25. https://doi.org/10.1038/nm.3954.
11. Russell PJ, Russell P, Rudduck C, Tse BW, Williams ED, Raghavan D. Establishing prostate cancer patient derived xenografts: lessons learned from older studies. Prostate. 2015;75:628–36. https://doi.org/10.1002/pros.22946.
12. Zhao H, Nolley R, Chen Z, Peehl DM. Tissue slice grafts: an in vivo model of human prostate androgen signaling. Am J Pathol. 2010;177:229–39. https://doi.org/10.2353/ajpath.2010.090821.
13. Zhao H, Thong A, Nolley R, Reese SW, Santos J, Ingles A, et al. Patient-derived tissue slice grafts accurately depict response of high-risk primary prostate cancer to androgen deprivation therapy. J Transl Med. 2013;11:199. https://doi.org/10.1186/1479-5876-11-199.
14. Wang Y, Revelo MP, Sudilovsky D, Cao M, Chen WG, Goetz L, et al. Development and characterization of efficient xenograft models for benign and malignant human prostate tissue. Prostate. 2005;64:149–59.
15. Priolo C, Agostini M, Vena N, Ligon AH, Fiorentino M, Shin E, et al. Establishment and genomic characterization of mouse xenografts of human primary prostate tumors. Am J Pathol. 2010;176:1901–13.
16. Lin D, Wyatt AW, Xue H, Wang Y, Dong X, Haegart A. et al. High fidelity patient-derived xenografts for accelerating prostate cancer discovery and drug development. Cancer Res. 2014;74:1272–83. https://doi.org/10.1158/0008-5472.CAN-13-2921-T.

17. Goldstein AS, Drake JM, Burnes DL, Finley DS, Zhang H, Reiter RE, et al. Purification and direct transformation of epithelial progenitor cells from primary human prostate. Nat Protoc. 2011;6:656–67.
18. Uronis JM, Osada T, McCall S, Yang XY, Mantyh C, Morse MA, et al. Histological and molecular evaluation of patient-derived colorectal cancer explants. PLoS One. 2012;7:e38422.
19. Kim MK, Osada T, Barry WT, Yang XY, Freedman JA, Tsamis KA, et al. Characterization of an oxaliplatin sensitivity predictor in a preclinical murine model of colorectal cancer. Mol Cancer Ther. 2012;11:1500–9.
20. Nguyen HM, Vessella RL, Morrissey C, Brown LG, Coleman IM, Higano CS, et al. LuCaP prostate cancer patient-derived xenografts reflect the molecular heterogeneity of advanced disease an-d serve as models for evaluating cancer therapeutics. Prostate. 2017;77:654–71.
21. Lawrence MG, Obinata D, Sandhu S. Patient-derived models of abiraterone- and enzalutamide-resistant prostate cancer reveal sensitivity to ribosome-directed therapy. Eur Urol. 2018;74:562–72. https://doi.org/10.1016/j.eururo.2018.06.020.
22. Li Q, Deng Q, Chao HP, Liu X, Lu Y, Lin K, et al. Linking prostate cancer cell AR heterogeneity to distinct castration and enzalutamide responses. Nat Commun. 2018;9:3600.
23. Pienta KJ, Abate-Shen C, Agus DB, Attar RM, Chung LWK, Greenberg NM, et al. The current state of preclinical prostate cancer animal models. Prostate. 2008;68:629–39.
24. Wise JP Sr, Wise SS, Little JE. The cytotoxicity and genotoxicity of particulate and soluble hexavalent chromium in human lung cells. Mutat Res. 2002;517:221–9.
25. Al-Alem U, Rauscher G, Shah E, Batai K, Mahmoud A, Beisner E, et al. Association of genetic ancestry with breast cancer in ethnically diverse women from Chicago. PLoS ONE. 2014;9:e112916.
26. Gupta S, Li J, Kemeny G, Bitting RL, Beaver J, Somarelli JA, et al. Whole genomic copy number alterations in circulating tumor cells from men with abiraterone or enzalutamide-resistant metastatic castration-resistant prostate cancer. Clin Cancer Res. 2017;23:1346–57. https://doi.org/10.1158/1078-0432.CCR-16-1211.
27. Andrews S. FastQC a quality control tool for high throughput sequence data. 2014. https://www.bioinformatics.babraham.ac.uk/projects/fastqc/.
28. Ewels P, Magnusson M, Lundin S, Kaller M. MultiQC: summarize analysis results for multiple tools and samples in a single report. Bioinformatics. 2016;32:3047–8.
29. Bolger AM, Lohse M, Usadel B. Trimmomatic: a flexible trimmer for Illumina sequence data. Bioinformatics. 2014;30:2114–20.
30. Dobin A, Davis CA, Schlesinger F, Drenkow J, Zaleski Z, Jha S, et al. STAR: ultrafast universal RNA-seq aligner. Bioinformatics. 2013;29:15–21.
31. Anders S, Pyl PT, Huber W. HTSeq-a Python framework to work with high-throughput sequencing data. Bioinformatics. 2015;31:166–9.
32. Anders S, Huber W. Differential expression analysis for sequence count data. Genome Biol. 2010;11:R106.
33. Benjamini Y, Hochberg Y. Controlling the false discovery rate - a practical and powerful approach to multiple testing. J R Stat Soc Ser B-Methodol. 1995;57:289–300.
34. Bass A, Storey J. qvalue: Q-value estimation for false discovery rate control. R (published bioinformatics package) package version 2.8.0, 2015. http://github.com/jdstorey/qvalue.
35. Haas B, Dobin A, Stransky N, Li B, Yang X, Tickle T, et al. STAR-fusion: fast and accurate fusion transcript detection from RNA-Seq. bioRxiv. 2017. https://doi.org/10.1101/120295.
36. Lagstad S. chimeraviz: visualization tools for gene fusions. R package version 1.10.0, 2019. https://www.bioconductor.org/packages/release/bioc/html/chimeraviz.html.
37. R Core Team. R: a language and environment for statistical computing. Vienna, Austria; R Core Team: 2019.
38. Gentlema R, Carey VJ, Bates DM, Bolstad B, Dettling M, Dudoit S, et al. Bioconductor: open software development for computational biology and bioinformatics. Genome Biol. 2004;5:R80.
39. Xie Y. Dynamic documents with R and knitr. 2nd ed. Boca Raton: CRC Press/Taylor and Francis; 2015. xxvii, 266.
40. Chang JT, Nevins JR. GATHER: a systems approach to interpreting genomic signatures. Bioinformatics. 2006;22:2926–33. https://doi.org/10.1093/bioinformatics/btl483.
41. Krämer A, Green J, Pollard J Jr, Tugendreich S. Causal analysis approaches in ingenuity pathway analysis. Bioinformatics. 2014;30:523–30.
42. Robinson D, Van Allen EM, Wu YM, Schultz N, Lonigro RJ, Mosquera JM, et al. Integrative clinical genomics of advanced prostate cancer. Cell. 2015;161:1215–28.
43. Zhu Z, Chung YM, Sergeeva O, Kepe V, Berk M, Li J, et al. Loss of dihydrotestosterone-inactivation activity promotes prostate cancer castration resistance detectable by functional imagingJ. Biol Chem. 2018;293:17829.
44. Leinonen KA, Saramäki OR, Furusato B, Kimura T, Takahashi H, Egawa S, et al. Loss of PTEN is associated with aggressive behavior in ERG-positive prostate cancer. Cancer Epidemiol Biomark Prev. 2013;22:2333–44.
45. Kregel S, Kiriluk KJ, Rosen AM, Cai Y, Reyes EE, Otto KB, et al. Sox2 is an androgen receptor-repressed gene that promotes castration-resistant prostate cancer. PLoS ONE. 2013;8:e53701.
46. Mu P, Zhang Z, Benelli M, Karthaus W, Hoover E, Chen C, et al. SOX2 promotes lineage plasticity and antiandrogen resistance in TP53- and RB1-deficient prostate cancer. Science. 2017;355:84–88. https://doi.org/10.1126/science.aah4307.
47. Lee M, Williams KA, Hu Y, Andreas J, Patel SJ, Zhang S, et al. GNL3 and SKA3 are novel prostate cancer metastasis susceptibility genes. Clin Exp Metastasis. 2015;32:769–82.
48. Magi-Galluzzi C, Tsusuki T, Elson P, Simmerman K, LaFargue C, Esgueva R, et al. TMPRSS2-ERG gene fusion prevalence and class are significantly different in prostate cancer of Caucasian, African-American and Japanese patients. Prostate. 2011;71:489–97.
49. Crea F, Quagliata L, Michael A, Liu H, Frumento P, Azad AA. et al. Integrated analysis of the prostate cancer small-nucleolar transcriptome reveals SNORA55 as a driver of prostate cancer progression. Mol Oncol. 2016;10:693–703. https://doi.org/10.1016/j.molonc.2015.12.010.
50. Rocha CRR, Silva MM, Quinet A, Cabral-Neto JB, Menck CFM. DNA repair pathways and cisplatin resistance: an intimate relationship. Clinics. 2018;73:e478s. https://doi.org/10.6061/clinics/2018/e478s.
51. Abida W, Cyrta J, Heller G, Prandi D, Armenia J, Coleman I. et al. Genomic correlates of clinical outcome in advanced prostate cancer. Proc Natl Acad Sci USA. 2019;116:11428–36. https://doi.org/10.1073/pnas.1902651116.
52. Xu L, Tang H, Wang K, Zheng Y, Feng J, Dong H, et al. Pharmacological inhibition of EZH2 combined with DNA-damaging agents interferes DNA damage response MM cells. Mol Med Rep. 2019;19:4249–55.
53. Zhan J, Wang P, Li S, Song J, He H, Wang Y. et al. HOXB13 networking with ABCG1/EZH2/Slug mediates metastasis and confers resistance to cisplatin in lung adenocarcinoma patients. Theranostics. 2019;9:2084–99. https://doi.org/10.7150/thno.29463. 76.
54. Qin X, Guo H, Wang X, Zhu X, Yan M, Wang X, et al. Exosomal miR-196a derived from cancer-associated fibroblasts confers cisplatin resistance in head and neck cancer through targeting CDKN1B and ING5. Genome Biol. 2019;20:12. https://doi.org/10.1186/s13059-018-1604-0.
55. Shen DW, Pouliot LM, Gillet JP, Ma W, Johnson AC, Hall MD, et al. The transcription factor GCF2 is an upstream repressor of the small GTPAse RhoA, regulating membrane protein trafficking, sensitivity to doxorubicin, and resistance to cisplatin. Mol Pharm. 2012;9:1822–33. https://doi.org/10.1021/mp300153z.
56. Street CA, Routhier AA, Spencer C, Perkins AL, Masterjohn K, Hackathorn A, et al. Pharmacological inhibition of Rho-kinase (ROCK) signaling enhances cisplatin resistance in neuroblastoma cells. Int J Oncol. 2010;37:1297–305. https://doi.org/10.3892/ijo_00000781.
57. Yu C, Wu G, Li R, Gao L, Yang F, Zhao Y, et al. NDRG2 acts as a negative regulator downstream of androgen receptor and inhibits the growth of androgen-dependent and castration-resistant prostate cancer. Cancer Biol Ther. 2015;16:287–96. https://doi.org/10.1080/15384047.2014.1002348.
58. Elvenes J, Thomassen EI, Johnsen SS, Kaino K, Sjøttem E, Johansen T. Pax6 represses androgen receptor-mediated transactivation by inhibiting recruitment of the coactivator SPBP. PloS One. 2011;6:e24659. https://doi.org/10.1371/journal.pone.0024659.
59. Shang Z, Niu Y, Cai Q, Chen J, Tian J, Yeh S. et al. Human kallikrein 2 (KLK2) promotes prostate cancer cell growth via function as a modulator to promote the ARA70-enhanced androgen receptor transactivation. Tumor Biol. 2014;35:1881–90. https://doi.org/10.1007/s13277-013-1253-6.
60. Patel R, Brzezinska EA, Repiscak P, Ahmad I, Mui E, Gao M, et al. Activation of β-catenin cooperates with loss of Pten to drive AR-independent castration-resistant prostate cancer. Cancer Res. 2020; 576–90. https://doi.org/10.1158/0008-5472.CAN-19-1684.
61. Nesbitt H, Browne G, O'Donovan KM, Byrne NM, Worthington J, McKeown SR. et al. Nitric oxide up-regulates RUNX2 in LNCaP prostate tumours: implications for tumour growth in vitro and in vivo. J Cell Physiol. 2016;23:473–82. https://doi.org/10.1002/jcp.25093.
62. Yang Y, Bai Y, He Y, Zhao Y, Chen J, Ma L. et al. PTEN loss promotes intratumoral androgen synthesis and tumor microenvironment remodeling via aberrant activation of RUNX2 in castration-resistant prostate cancer. Clin Cancer Res. 2018;24:834–46. https://doi.org/10.1158/1078-0432.CCR-17-2006.
63. Ozaki T, Yu M, Yin D, Sun D, Zhu Y, Bu Y, et al. Impact of RUNX2 on drug-resistant human pancreatic cancer cells with p53 mutations. BMC Cancer. 2018;18:309. https://doi.org/10.1186/s12885-018-4217-9.
64. Yu L, Su YS, Zhao J, Wang H, Li W. Repression of NR4A1 by a chromatin modifier promotes docetaxel resistance in PC-3 human prostate cancer cells. FEBS Lett. 2013;587:2542–51.
65. Elkin M, Vlodavsky I. Tail vein assay of cancer metastasis. Curr Protoc Cell Biol. 2001. https://doi.org/10.1002/0471143030.cb1902s12.

ACKNOWLEDGEMENTS

We acknowledge the BioRepository & Precision Pathology Center (BRPC), a shared resource of the Duke University School of Medicine and Duke Cancer Institute, for providing access to the human biospecimens used under Institutional Review Board oversight in this work, the assistance of the Duke University Health System Clinical Molecular Diagnostics Laboratory, Duke Sequencing and Genomic Technologies Shared Resource, and the Duke Cancer Institute Bioinformatics Shared Resource, and Bonnie LaCroix, laboratory manager. Support: P30 Cancer Center Support Grant (P30 CA014236), NIH Basic Research in Cancer Health Disparities R01 Award R01CA220314 to SRP PI, JAF and DSH Co-I, DJG and KO Collaborator, WCF Pathologist.

AUTHOR CONTRIBUTIONS

BMP: Conceptualization, Investigation, Formal Analysis, Writing, Visualization; WCF: Investigation, Formal Analysis, Writing, Visualization; TA: Formal Analysis, Writing, Visualization; JAS: Methodology, Writing; KEW: Methodology, Writing; SG: Investigation, Formal Analysis, Writing, Visualization; SW: Investigation, Formal Analysis, Writing, Visualization; JPW: Methodology, Writing; XQ: Formal Analysis, Writing, Visualization; DZ: Formal Analysis, Writing, Visualization; LX: Methodology; YL: Methodology; XC: Methodology; BAI: Conceptualization, Resources, Writing; SJM: Resources, Writing; JH: Conceptualization, Writing; RAK: Investigation, Formal Analysis, Writing, Visualization; KO: Conceptualization, Validation, Writing; SG: Conceptualization, Validation, Writing; AJA: Conceptualization, Writing; DJG: Conceptualization, Writing; SRP: Conceptualization, Writing, Supervision, Funding Acquisition; DSH: Conceptualization, Writing, Supervision, Project Administration, Funding Acquisition; JAF: Conceptualization, Writing, Supervision, Project Administration, Funding Acquisition.

COMPETING INTERESTS

The authors declare no competing interests.

ADDITIONAL INFORMATION

Supplementary information The online version contains supplementary material available at https://doi.org/10.1038/s41391-021-00460-y.

Correspondence and requests for materials should be addressed to Jennifer A. Freedman.